

Research Article

Spatio-Temporal Assessment of Surface Albedo using Landsat 8 Images in Lalgudi Block of Trichy District, Tamil Nadu

J. RAMACHANDRAN^{1*}, R. LALITHA², K. SIVASUBRAMANIAN³ AND S. VALLAL KANNAN⁴

¹Department of Agricultural Engineering, Agricultural College and Research Institute, Tamil Nadu Agricultural University (TNAU), Madurai-625104, Tamil Nadu

²Department of Soil and Water Conservation Engineering, Agricultural Engineering College and Research Institute, TNAU, Kumulur-621712, Trichy, Tamil Nadu

³Office of Controller of Examination, TNAU, Coimbatore-641003, Tamil Nadu

⁴Department of Irrigation and Drainage Engineering, Agricultural Engineering College and Research Institute, TNAU, Kumulur-621712, Trichy, Tamil Nadu

ABSTRACT

Satellite remote sensing is an essential technique for estimating land surface albedo at various spectral, spatial and temporal resolutions. It has continuously improved during the past three decades, and many satellite products are now available for modelling surface albedo. In this paper surface albedo was computed from OLI-TIRS Landsat 8 data products in Lalgudi block of Tiruchirapalli district, Tamil Nadu, India. The study was conducted for two growing seasons (2017-19) with eleven Landsat 8 images that were downloaded from USGS earthexplorer website. In the scenes having cloud cover, the maximum surface albedo values (0.7 to 0.8) were found. The values obtained for surface albedo of sand in river bed was around 0.4 and for water was around 0.03. The surface albedo for barren land and lush vegetation present in northern part ranges from 0.2 to 0.3 and 0.12 to 0.23, respectively. Results indicated that, surface albedo values for settlements varied between 0.12 to 0.23. The surface albedo gave a clear indication of sand, water, settlements and cultivated lands which helps in demarcation and differentiation of different land uses.

Key words: Remote sensing, surface albedo, Landsat 8 image

Introduction

Land surface albedo is widely used in climate and environment applications. It is the proportion of solar energy reflected back by the earth's surface. There is an increasing need for albedo data to be available for use in wide applications that require a fine spatial resolution of satellite images. The main way to obtain continuous surface albedo for large areas is satellite remote sensing. Researchers started

obtaining surface albedo from different satellite images (Hong *et al.*, 2009). Remote sensing based algorithms with multi-spectral high-resolution satellite data has become a strong tool for estimation of spatial and temporal variation in surface albedo.

Remote sensing and GIS techniques helps in arriving at an action plan for sustainable development. Kar *et al.* (2019) stated that remote sensing and GIS techniques are employed to assess impact of technology over large areas and remote sensing images can be compared before and after

*Corresponding author,
Email: eesurya.tnau@gmail.com

the technological interventions. Kar *et al.* (2020) demonstrated the capability of remote sensing and GIS techniques for developing sustainable land use system on watershed basis.

Several studies had been presented for surface albedo estimation from different satellite data using different methodologies. Schaaf *et al.* (2000) presented the algorithm and preliminary results of the Moderate Resolution Imaging Spectroradiometer (MODIS) bidirectional reflectance distribution function (BRDF). Liang (2000) obtained equations that allow calculating the albedo through the linear combination of the monochromatic reflectivity of each one of these bands in the solar radiation domain for various orbital sensors. Liang (2003) presented a direct algorithm for estimating land surface broadband albedos from MODIS imagery. Mokhtari and Busu (2011) explored the capability of advanced spaceborne thermal emission and reflection radiometer's (ASTER), VNIR (visual and near infrared) and SWIR (shortwave infrared) spectral bands (except thermal bands) in estimating surface albedo using statistical approach. da Silva *et al.* (2016) presented an elaborate procedure for computing surface albedo from Landsat 8 Operational Land Imager (OLI) images. The albedo obtained with OLI images provides more significant degree of differentiation in land use/cover classification due to increased radiometric resolution

of sensors in Landsat 8 (da Silva *et al.*, 2016).

Landsat 8 is a science mission satellite that carries two sensors namely: Operational Land Imager (OLI) and Thermal Infrared Sensor (TIRS) launched on February 11, 2013 by NASA (National Aeronautics and Space Administration). This incorporates improved performance of Landsat 8 over the other Landsat missions (Roy *et al.*, 2014). Due to free access to Landsat data and recent technical advancements in data processing, there is the potential for albedo data to be used in different applications, such as calculation of earth's surface energy (Liaqat and Choi, 2015), water balance studies (Semmens *et al.*, 2016) and helps in identifying land use/cover changes, urban environmental assessment (Zhou *et al.*, 2012), agricultural monitoring (Gao *et al.*, 2014; Li and Fang, 2015), forestry management (Kuusinen *et al.*, 2014; Vanderhoof *et al.*, 2014), and ecosystem functioning evaluation (Lagomasino *et al.*, 2015). Surface albedo cannot be directly obtained from the Landsat 8 image.

Hence to explore the potential of surface albedo applications that was determined using recent images from OLI, this study was taken up. This study aimed to compute surface albedo for different land use/cover from OLI-TIRS Landsat 8 data products in Lalgudi block, Tiruchirapalli district, Tamil Nadu, India.

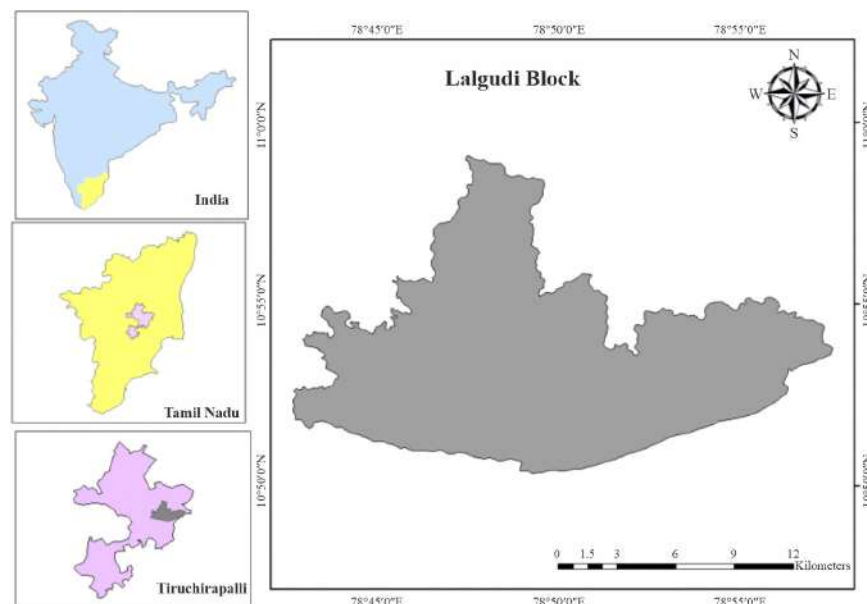


Fig. 1. Study area – Lalgudi block of Trichy district, Tamil Nadu

Materials and Methods

Study area

Lalgudi block, located at Tiruchirapalli District, Tamil Nadu, India was selected for this study. The geographical location of Lalgudi block is shown in Fig. 1. Lalgudi block is situated between $10^{\circ}59'1.83''$ N and $10^{\circ}50'22.94''$ N latitudes and $78^{\circ}42'50.19''$ E and $78^{\circ}57'39.95''$ E longitudes and located 70 m above mean sea level. The northern part of Lalgudi block has dense vegetation and barren lands. The southern part is bounded by the river Coleroon, Panguni river and Pullambadi canal flow through Lalgudi block. The total geographical area of the block is 20558 hectares. Lalgudi town is located at the central part of the block. Agriculture is the main occupation of Lalgudi block. Around 45 percent of area in Lalgudi block is used for agriculture. Most of the inner part of the Lalgudi block has cultivated areas where paddy, sugarcane, banana and other vegetables are grown. In Lalgudi block, 90 percent

of the crop production is done by irrigation and the remaining 10 percent is under rainfed cropping.

Selection of landsat 8 images

The study was conducted for two growing seasons (2017-19). Hence, eleven Landsat 8 images were acquired over the growing seasons. Landsat images were downloaded from USGS website (<https://earthexplorer.usgs.gov/>). The image acquisition date, solar elevation angle and zenith angle for the Landsat 8 data products used in this study are given in Table 1. The images were selected such that there is no or minimum cloud cover in order to avoid error in calculation.

Estimation of surface albedo (α)

Surface albedo (α) is defined as the amount of radiation reflected back by the surface. It was estimated as the ratio of difference between planetary albedo (α_{toa}) and atmospheric albedo (α_{atm}) of each pixel to the square of atmospheric transmittance (τ).

Table 1. Multiplicative and Additive factors used in calculation of radiance

Date	Variables	Band 2	Band 3	Band 4	Band 5	Band 6	Band 7
2017-08-07	Mult _{rad}	1.25E-02	1.15E-02	9.71E-03	5.94E-03	1.47E-03	4.98E-04
	Add _{rad}	-62.5126	-57.6048	-48.5756	-29.7258	-7.3925	-2.4916
2017-10-10	Mult _{rad}	1.28E-02	1.18E-02	1.00E-02	6.13E-03	1.52E-03	5.13E-04
	Add _{rad}	-64.4722	-59.4106	-50.0983	-30.6577	-7.6242	-2.5697
2017-12-29	Mult _{rad}	1.33E-02	1.23E-02	1.03E-02	6.32E-03	1.57E-03	5.30E-04
	Add _{rad}	-66.4792	-61.2600	-51.6579	-31.6121	-7.8616	-2.6497
2018-01-30	Mult _{rad}	1.33E-02	1.22E-02	1.03E-02	6.30E-03	1.57E-03	5.28E-04
	Add _{rad}	-66.2511	-61.0498	-51.4807	-31.5036	-7.8346	-2.6407
2018-03-03	Mult _{rad}	1.30E-02	1.20E-02	1.01E-02	6.22E-03	1.54E-03	5.21E-04
	Add _{rad}	-65.4237	-60.2874	-50.8377	-31.1101	-7.7368	-2.6077
2018-05-22	Mult _{rad}	1.25E-02	1.15E-02	9.75E-03	5.96E-03	1.48E-03	5.00E-04
	Add _{rad}	-62.7401	-57.8144	-48.7524	-29.8340	-7.4194	-2.5007
2018-09-11	Mult _{rad}	1.26E-02	1.16E-02	9.85E-03	6.03E-03	1.50E-03	5.05E-04
	Add _{rad}	-63.4195	-58.4406	-49.2804	-30.1571	-7.4998	-2.5278
2018-11-14	Mult _{rad}	1.31E-02	1.21E-02	1.02E-02	6.24E-03	1.55E-03	5.23E-04
	Add _{rad}	-65.6678	-60.5123	-51.0274	-31.2262	-7.7656	-2.6174
2019-01-01	Mult _{rad}	1.32E-02	1.22E-02	1.03E-02	6.32E-03	1.57E-03	5.30E-04
	Add _{rad}	-66.4871	-61.2673	-51.6640	-31.6158	-7.8625	-2.6501
2019-03-06	Mult _{rad}	1.30E-02	1.20E-02	1.01E-02	6.21E-03	1.54E-03	5.20E-04
	Add _{rad}	-65.3292	-60.2003	-50.7643	-31.0652	-7.7256	-2.6039
2019-05-09	Mult _{rad}	1.26E-02	1.16E-02	9.80E-03	6.00E-03	1.49E-03	5.02E-04
	Add _{rad}	-63.0908	-58.1376	-49.0249	-30.0008	-7.4609	-2.5147

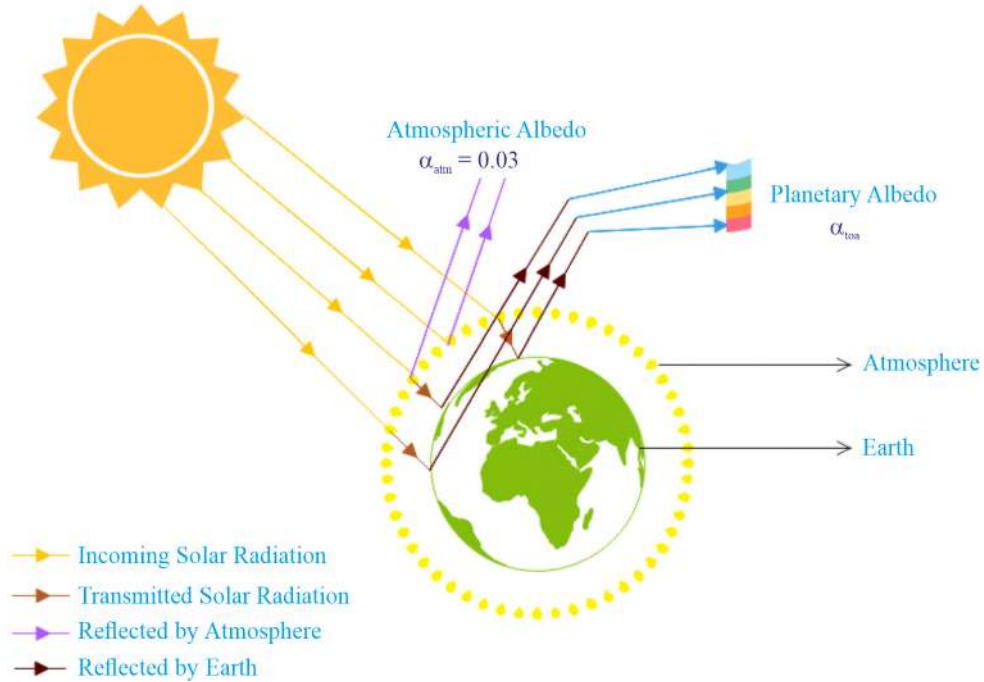


Fig. 2. Representation of atmospheric and planetary albedo

A detailed representation of atmospheric and planetary albedo is shown in Fig. 2. The equation is as follows:

$$\alpha = \frac{(\alpha_{\text{toa}} - \alpha_{\text{atm}})}{\tau^2} \quad \dots(1)$$

The atmospheric transmittance is a function of elevation and was computed using the following equation (Waters *et al.*, 2002):

$$\tau = 0.75 + (0.00002 * z) \quad \dots(2)$$

Where z is the elevation raster extracted for the study area from digital elevation model (DEM). The Shuttle Radar Topographic Mission (SRTM) DEM downloaded from the USGS EarthExplorer website was used in this calculation.

The atmospheric albedo ranges from 0.025 to 0.040. An average value of 0.03 was taken for the atmospheric albedo i.e. three percent of solar radiation is reflected back by the atmosphere (Bastiaanssen *et al.*, 1998).

The planetary albedo or albedo without correction was estimated from the six different bands (2, 3, 4, 5, 6, 7) of Landsat 8 dataset. Firstly, the radiance (\tilde{n}_b) was calculated from the pixel values of

different bands (DN_b) using the following equation:

$$\rho_b = Add_{\text{rad},b} + (Mult_{\text{rad},b} * DN_b) \quad \dots(3)$$

where $Add_{\text{rad},b}$ is additive and $Mult_{\text{rad},b}$ is multiplicative terms related to different band radiance. The values were obtained from the metadata text file downloaded along with each dataset and presented in Table 1.

Then, the reflectance of each band was obtained from the following equation:

$$r_b = \frac{[Add_{\text{ref},b} + (Mult_{\text{ref},b} * DN_b)]}{\cos z * d_r} \quad \dots(4)$$

where $Add_{\text{ref},b}$ is additive and $Mult_{\text{ref},b}$ is multiplicative terms related to different band reflectance obtained from the metadata text file. The angle z is called sun zenith angle which is 90 minus sun elevation angle. The elevation angle was obtained from the metadata text file.

The d_r corresponds to the correction of the eccentricity of the terrestrial orbit, which is given by

$$d_r = \left(\frac{1}{d_{\text{ES}}} \right)^2 \quad \dots(5)$$

Table 2. Variables used in albedo calculation

Acquisition Date (yyyy/mm/dd)	Solar Zenith Angle (degrees)	Mult _{ref}	Add _{ref}	d _{ES} (AU)
2017-08-07	26.30	0.00002	-0.1	1.01408
2017-10-10	28.46	0.00002	-0.1	0.99855
2017-12-29	42.92	0.00002	-0.1	0.98336
2018-01-30	40.61	0.00002	-0.1	0.98505
2018-03-03	33.62	0.00002	-0.1	0.99126
2018-05-22	25.25	0.00002	-0.1	1.01224
2018-09-11	25.22	0.00002	-0.1	1.00680
2018-11-14	36.47	0.00002	-0.1	0.98942
2019-01-01	42.99	0.00002	-0.1	0.98330
2019-03-06	32.94	0.00002	-0.1	0.99198
2019-05-09	24.36	0.00002	-0.1	1.00942

where d_{ES} is the Earth-to-Sun distance in astronomic unit (AU) for each selected days which was also obtained from the meta data test file. The Add_{ref,b}, Mult_{ref,b}, solar zenith angle and Earth to Sun distance of different Landsat 8 dataset is listed in Table 2.

Next, the solar constant K_b (W m⁻² μm) for each bands was calculated from the following equation:

$$K_b = \frac{\pi * \rho_b}{r_b * \cos z * d_r} \quad \dots(6)$$

where all the terms were estimated in the earlier steps for each bands. Then the albedo weights (p_b) were obtained from K_b raster by using the following expression:

$$P_b = \frac{K_b}{K_{sum}} \quad \dots(7)$$

where K_{sum} is the sum of K_b values of different bands used in calculation. Finally, the planetary albedo was estimated as the summation of product of albedo weight and reflectance of the different bands used in the calculation. The expression for planetary albedo estimation is given by

$$\alpha_{toa} = \sum_{b=2}^7 p_i * r_i \quad \dots(8)$$

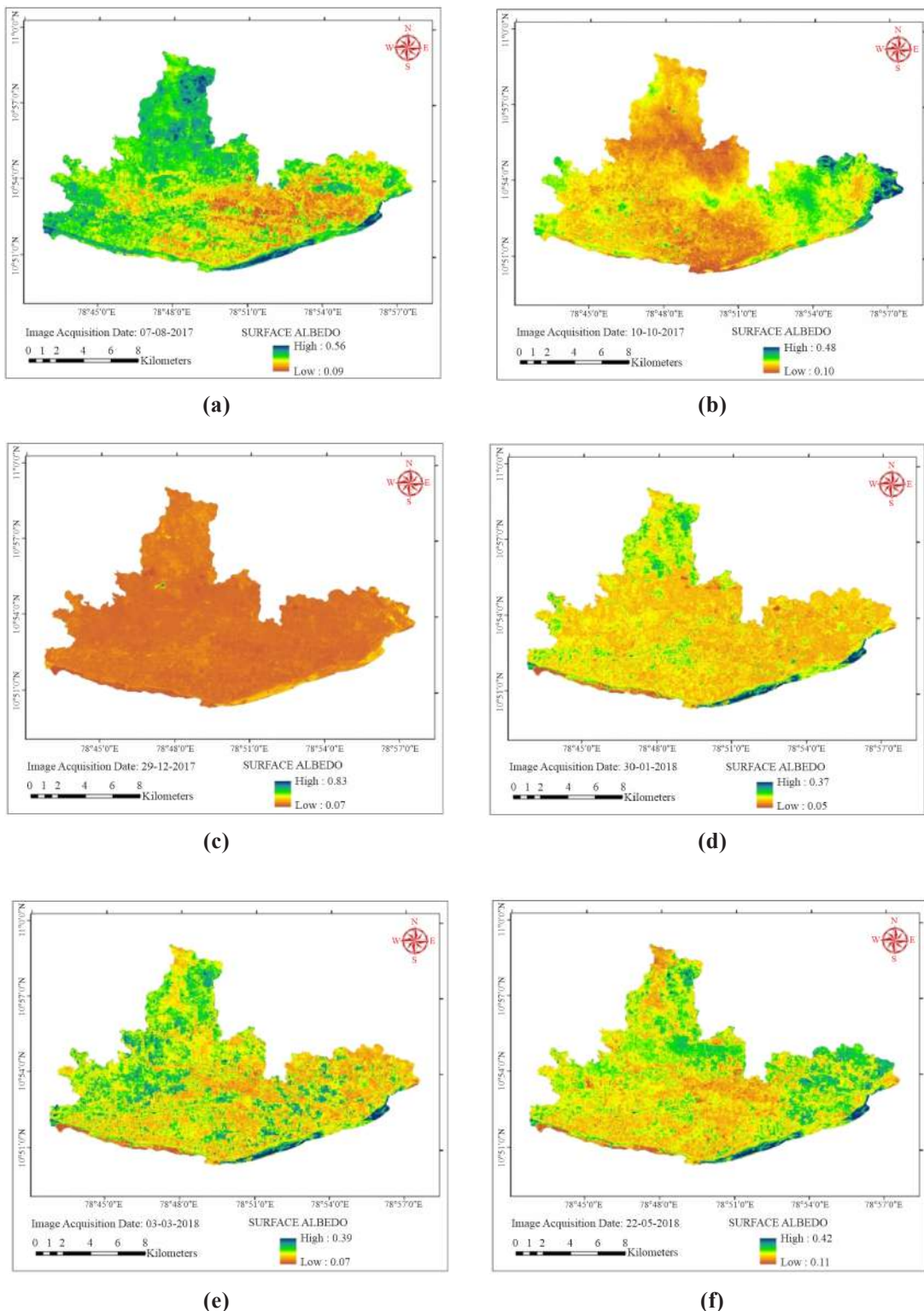
By substituting in Eq. (1), the surface albedo raster was obtained. All the calculations were done using Raster Calculator tool in ArcGIS 10.2.

Results and Discussion

The spatial and temporal variation of surface albedo in the study area were obtained from SEBAL model for the eleven selected scenes (Fig. 3). In the scenes having cloud cover, the maximum surface albedo values (0.7 to 0.8) were found. In scene taken during 01-01-2019, the patches of dense cloud has very high surface albedo value (1.42) whereas the shadow of the clouds had very less value (0.07). Similarly, da Silva *et al.* (2016) also reported that in the pixels corresponding to the clouds, the albedo was generally higher than 80% and, in areas shaded by the clouds, the values were lower than those of water, which is due to the method of calculation of the incident solar radiation in each pixel.

The surface albedo values obtained in the south-eastern part of the study area ranges from 0.20 to 0.37. This indicates the presence of dry sand in River Coleroon. Similarly, the surface albedo values of south-western part varied from 0.05 to 0.10 which indicates the standing water in the flow path of River Coleroon. The values obtained were consistent with those values reported in literature for surface albedo of sand (0.4) and water (0.03). Faris *et al.* (2016) also reported a mean value of 0.05 for water bodies.

The surface albedo for barren land and lush vegetation present in northern part ranges from 0.2 to 0.3 and 0.12 to 0.23, respectively. Allen *et al.* (1998) also reported average albedo values for vegetation as 0.23. The image acquisition dates



Contd...

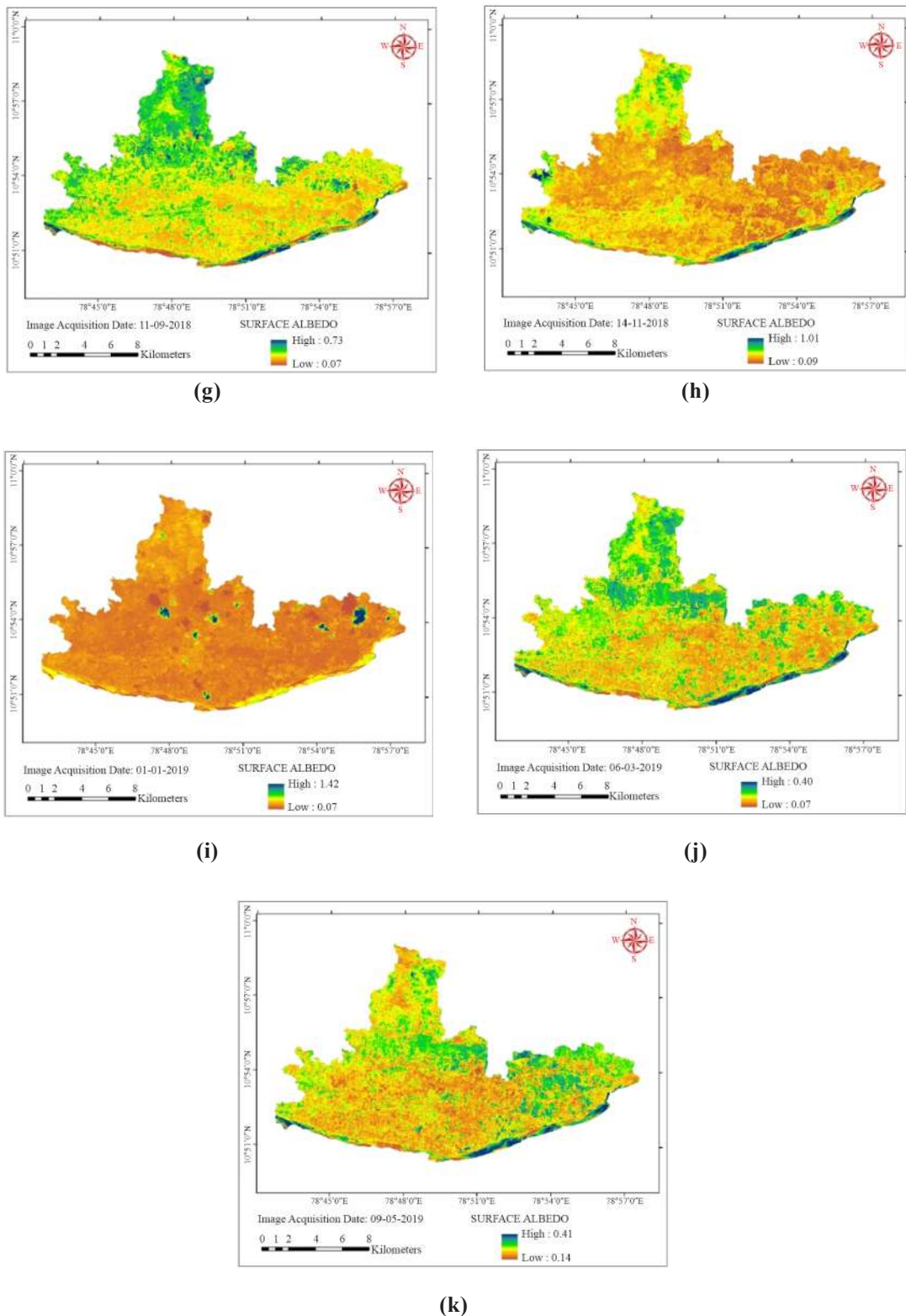


Fig. 3. Variation of surface albedo of Lalgudi block

falling in initial stage of samba season showed surface albedo values around 0.05 which indicates the puddled paddy fields with standing water that has less surface albedo. The images of further dates showed increasing trend in albedo due to the coverage of crops. The settlements and buildings is clearly demarcated in the central part of the town with surface albedo values ranging from 0.15 to 0.20 which is similar to the results reported in Spångmyr (2010). Faris *et al.* (2016) also reported mean value of 0.15 for buildup areas. The results were consistent with that of surface albedo values reported by Salifu and Agyare (2012) for water bodies, barren lands, built up area and farm lands. The surface albedo gave a clear indication of sand, water, settlements and cultivated lands which helps in demarcation and differentiation of different land uses.

Conclusion

Surface albedo is an important parameter for controlling the surface energy budget. Satellite albedo products at fine resolution allow for applications such as agricultural monitoring, urban environment assessment, and forest management; therefore, the demand for these products is increasing. Hence the surface albedo maps generated in this study for the block will be highly useful in studying the relation between surface albedo, land use, climate, soil and water resources.

References

- Allen, R.G., Pereira, L.S. , Raes, D. and Smith, M. 1998. Crop evapo-transpiration: Guidelines for computing crop water requirements. Rome: Food and Agricultural Organization.
- da Silva, B.B., Braga, A.C., Braga, C.C., de Oliveira, L.L.M., Montenegro, S.M.G.L. and Junior, B.B. 2016. Procedures for calculation of the albedo with OLI-Landsat 8 images: Application to the Brazilian semi-arid. *Revista Brasileira de Engenharia Agrícola e Ambiental*. **20(1)**: 3-8.
- Faris, A.A., Beg, H., Ahmed, A.S., Adrian, O., Anna, J. and Adriana, M. 2016. Estimation of evapotranspiration using SEBAL Algorithm and Landsat-8 Data—A case study: Tatra Mountains Region. *Journal of Geological Resource and Engineering* **4(6)**.
- Gao, F., He, T., Masek, J.G., Shuai, Y.M., Schaaf, C.B. and Wang, Z.S. 2014. Angular effects and correction for medium resolution sensors to support crop monitoring. *IEEE J. Sel. Top. Appl. Earth Obs. Remote. Sens.* **7**: 4480-4489.
- Hong, S.H., Hendrickx, J.M.H. and Borchers, B. 2009. Up-scaling of SEBAL derived evapotranspiration maps from LANDSAT (30 m) to MODIS (250 m) scale. *J. Hydrol.*, **370(1-4)**: 122-138.
- Kar, G., Anand, P.S.B., Raychoudhuri, M., Panda, D.K., Sahoo, H.M., Nayak, S.R., Dora, K.R., Patra, P.K., Sahoo, N., Kumar, A. and Ambast, S.K. 2019. Determining digital elevation model (DEM), slope and impact analysis of water management interventions in coastal seasonal waterlogged areas using remote sensing and GIS. *Journal of Agricultural Physics* **19(2)**: 176-184.
- Kar, G., Chaudhari, S.K., Patra, P.K., Dixit, P.R. and Alam, N.M. 2020. GIS based sustainable land use planning using spatial variation of soil and terrain information. *Journal of Agricultural Physics* **20(1)**: 15-21.
- Kuusinen, N., Tomppo, E., Shuai, Y. and Berninger, F. 2014. Effects of forest age on albedo in boreal forests estimated from MODIS and Landsat albedo retrievals. *Remote Sens. Environ.* **145**: 145-153.
- Lagomasino, D., Price, R.M., Whitman, D., Melesse, A. and Oberbauer, S.F. 2015. Spatial and temporal variability in spectral-based surface energy evapotranspiration measured from Landsat 5TM across two mangrove ecotones. *Agric. For. Meteorol.* **213**: 304-316.
- Li, W.J. and Fang, H.L. 2015. Estimation of direct, diffuse, and total FPARs from Landsat surface reflectance data and ground-based estimates over six FLUXNET sites. *J. Geophys. Res. Biogeosci.* **120**: 96-112.
- Liang, S. 2000. Narrowband to broadband conversions of land surface albedo I Algorithms. *Remote Sensing of Environment* **76**: 213-238.
- Liang, S. 2003. A direct algorithm for estimating land surface broadband albedos from MODIS imagery. *IEEE Trans. Geosci. Remote Sens.* **41**: 136-145.
- Liaqat, U.W. and Choi, M. 2015. Surface energy fluxes in the Northeast Asia ecosystem: SEBS

- and METRIC models using Landsat satellite images. *Agricultural and Forest Meteorology* **214-215**: 60–79.
- Mokhtari, H.M. and Busu, I. 2011. Downscaling Albedo from moderate-resolution imaging spectroradiometer (MODIS) to advanced spaceborne thermal emission and reflection radiometer (ASTER) over an agricultural area utilizing ASTER visible-near infrared spectral bands. *International Journal of the Physical Sciences* **6(24)**: 5804-5821.
- Roy, D.P., Wulder, M.A., Loveland, T.R., Woodcock, C.E., Allen, R.G., Anderson, M.C., Helder, D., Irons, J.R., Johnson, D.M., Kennedy, R., Scambos, T.A., Schaaf, C.B., Schott, J.R., Sheng, Y., Vermote, E.F., Belward, A.S., Bindschadler, R., Cohen, W.B., Gao, F., Hippel, J.D., Hostert, P., Huntington, J., Justice, C.O., Kilic, A., Kovalskyy, V., Lee, Z.P., Lymburner, L., Masek, J.G., McCorkel, J., Shuai, Y., Trezza, R., Vogelmann, J., Wynne, R.H. and Zhu, Z. 2014. Landsat-8: Science and product vision for terrestrial global change research. *Remote Sensing of Environment* **145**: 154-172.
- Salifu, T. and Agyare, W.A. 2012. Distinguishing Land use types using Surface Albedo and Normalized Vegetative Index Derived from the SEBAL Model for the Atankwidi and Afram Sub-Catchments in Ghana. *ARPN Journal of Engineering and Applied Sciences*. **7(1)**: 69-80.
- Semmens, K.A., Anderson, M.C., Kustas, W.P., Gao F., Alfieri, J.G., McKee, L., Prueger, J.H., Hain, C.R., Cammalleri, C., Yang, Y., Xia, T., Sanchez, L., Alsina, M.M. and Vélez, M. 2016. Monitoring daily evapotranspiration over two California vineyards using Landsat 8 in a multi-sensor data fusion approach. *Remote Sensing of Environment* **185**: 155–170.
- Schaaf, C., Gao, F., Strahler, A., Lucht, W., Li, X., Tsang, T., Strugnell, N., Zhang, X., Jin, Y. and Muller, J. 2002. First operational BRDF, albedo nadir reflectance products from MODIS. *Remote Sens. Environ.*, **83**: 135–148.
- Spångmyr, M. 2010. Global effects of albedo change due to urbanization. Edited by Department of Earth and Ecosystem Sciences. Sweden: Division of Physical Geography and Ecosystems Analysis. Lund University.
- Vanderhoof, M., Williams, C.A., Shuai, Y., Jarvis, D., Kulakowski, D. and Masek, J. 2014. Albedo-induced radiative forcing from mountain pine beetle outbreaks in forests, south-central Rocky Mountains: magnitude, persistence, and relation to outbreak severity. *Biogeosciences* **11**: 563-575.
- Waters, R., Allen, R., Tasumi, M., Trezza, R. and Bastiaanssen, W. 2002. Surface Energy Balance Algorithms for Land: Advanced Training and User's Manual. 1-98.
- Zhou, Y.Y., Weng, Q.H., Gurney, K.R., Shuai, Y.M. and Hu, X.F. 2012. Estimation of the relationship between remotely sensed anthropogenic heat discharge and building energy use. *ISPRS J. Photogramm. Remote Sens.* **67**: 65-72.

Received: August 17, 2021; Accepted: November 22, 2021